Kinetic sheath in presence of multiple positive ions, negative ions and particle wall emission

L. Schiesko,[a] D. Wünderlich, and I. M. Montellano
Max-Planck-Institut für Plasmaphysik, Boltzmannstrasse 2, D-85748 Garching, Germany.

(Dated: 4 December 2019)

The region between a Maxwellian plasma source and a floating or current-carrying surface is described by a static, one-dimensional collisionless kinetic sheath model. In the plasma source, electrons, negative ions and several positive ion species with different temperatures can be included. The surface (wall) can emit electrons and/or negative ions. When the flux of surface-emitted negative ions and/or electrons reaches a critical value, the sheath becomes space-charge saturated which leads to the formation of a virtual cathode in front of the emitting wall and set the maximum current density that can be transported from the surface to the plasma. The analytical results are benchmarked against a particle-in-cell code.

I. INTRODUCTION

In plasma reactors, the plasma-sheath acts as a transition between the plasma and the walls[1–4]. Because it is a non-Maxwellian and non-neutral region, it has a substantial influence on the particle and energy transport to a plasma-facing component. For example, depending on the particle energy impinging the wall and its intrinsic properties, secondary electron emission cannot be neglected and has to be accounted for[5–11]. In another example, large currents of negative hydrogen ions generated on caesiated surfaces are extracted from hydrogen ion sources[12–14]. For both secondary electrons and negative ions, when the wall emission reaches a critical value (and beyond), a virtual cathode near the wall is formed, limiting either the secondary electron[15–19] or negative ion[20,21] current that can be transported from the wall towards the plasma. When this is the case, the sheath is space-charge saturated and will be labelled in the following by the term critical regime, while the term sub-critical will be used otherwise.

Particle-in-cell simulations are able to model accurately the plasma-sheath including secondary electron or negative ion emission but are time consuming, in particular those including two or three spatial dimensions. The execution time of one spatial dimension particle-in-cell simulation can be of several hours if many particle species with different masses or high densities in the plasma bulk and/or surface emission have to be included. They are thus not suited if parameters scans have to be used to find trends. Conversely, analytical models can solve tens of different cases with a time scale in the order of the second. For this reason, it is very desirable to develop or extend, as done in this paper, an analytical model capable to solve sheath potential and density profiles of multiple plasma and surfaces-emitted species.

The presented results were obtained from a fully kinetic treatment of the plasma and wall-emitted particles. It is based on the use of a cut-off particle energy leading to truncated velocity distribution functions for all the involved species i.e. source and wall emitted particles. The use of this formalism to describe sheaths was started by the work of authors such as Auer[22] and McIntyre[23] and further developed by Kuhn[24]. Schwager[16,25] extended the model to allow unequal plasma ion and electron temperatures and to take into account secondary electron emission (SEE) from a floating wall, while the work done by Ordonez[17,18] permitted to model current carrying sheaths with SEE values larger than critical emission.

When considering particles in an accelerating potential such as positive ions travelling from the plasma towards a wall, the minimum velocity that possess the positive ions increases with the local accelerating potential, leading to a truncated velocity distribution function. The same reasoning holds for wall-emitted electrons or negative ions, with the exception that they are travelling from the wall towards the plasma and thus all the particles reach the plasma. In the case of particles in a retarding potential like electrons from the plasma directed toward a wall, most of them will be returned towards the plasma bulk, while the ones with the largest velocity will hit the wall. The electrons hitting the wall are lost, truncating the velocity distribution function. The use of a cut-off particle energy produces erf(ϕ) density profiles, ϕ being the potential and erf(x) the error function, in contrast to the exp(ϕ) (Boltzmann factor) dependence found without cut-off[15,20,26–28].

The following results are based on an extension of the work of Ordonez[17,18]. The main goal of this paper is to derive the generalized analytical expressions for a plasma containing, in the bulk, multiple positive ion species, electrons and negative ions, in contact with a surface able to emit secondary electrons and negative ions.
In section II and for completeness, the standard assumptions will be recalled together with the expressions for phase-space distribution functions and associated densities, fluxes, normalized temperatures, and energy fluxes for the two potential energy profiles in Fig. 1. These expressions are used in section III to evaluate numerically the potential profiles. In section IV are given details of a particle-in-cell (PIC) code for negative ions, while a comparison between the presented model and the PIC code is made in section V. In section VI, some results showing how the source and wall potentials

[a]Electronic mail: loic.schiesko@ipp.mpg.de

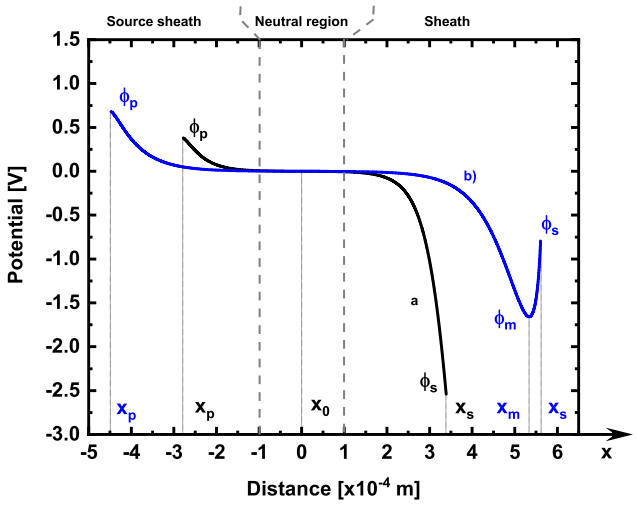

FIG. 1. Curve a) represents the potential profile computed for a floating surface located at the position x_s with the potential ϕ_s, a plasma made of electrons with $T_e = 1$ eV, and H^+ ions with $T_H^+ = 0.8$ eV injected at the location x_p with the potential ϕ_p. Curve a) is an example of sub-critical regime. Curve b) represents the potential profile computed for a floating surface with the same electron and H^+ temperature as in a) with H^- injected at ϕ_s with $\delta_H^- = 3$ and $T_H^- = 0.5$ eV and is an example of critical regime. ϕ_m corresponds to the potential minimum achieved in presence of surface negative ion emission. x_0 is the sheath-source sheath interface, for which the potential value is set to zero. The location of the plasma and wall particle sources are x_p and x_s respectively.

as well as the particle fluxes are affected by the secondary electron emission and negative ion yield will be shown. Finally a short discussion is made in section VII on the results presented here and the Campanell's inverse sheath theory[29,30].

II. PLANAR SOURCE MODEL

A. General considerations

The plasma in the vicinity of a solid surface material can be divided into three regions as shown in Fig. 1. The potential profiles presented in Fig. 1 were computed for half-Maxwellian equal fluxes of negative and positive charges injected in the source located at the position x_p with a potential ϕ_p. When considering for example only electrons and positive ions in the source, the mass difference between electrons and positive ions is responsible for a velocity difference and thus, the net charge density is not zero at ϕ_p. Consequently, a source sheath develops in order to decelerate the electrons and accelerate the ions in order to recover the charge density neutrality over a few Debye lengths typically (neutral region in Fig. 1).
The second region is the neutral region and is located between the source sheath and the sheath. At each location within this region the total charge density is zero. All the species in the neutral region have a non-Maxwellian velocity distribution function because of the source sheath or sheath potential drops for the particles injected in the source or at the wall respectively, in contrast to the sheaths formalisms developed here[20] or there[36] which assume a Maxwellian distribution in the neutral region for the plasma species.
The last region is the sheath between the wall and the neutral region, which is a non-neutral and non-Maxwellian region. In the case of a floating wall for example, the fluxes of electrons and positive ions are strictly equal at the wall.

In this paper, source-emitted negative charges which are repelled by the electric field, as well as the wall-emitted negative charges, reach the source location with a negative-x velocity where they are added to the injected flux with the temperature of the source electrons as explained in[25]. This condition avoids the accumulation of negative charges in the source and enforces the zero electric field condition at x_p.
This particle injection method has been extensively discussed by Procassini[31] and benchmarked against the work of Emmert[32], Bissel and Johnson[33], Scheuer and Emmert[34] (the three authors considering a variable positive ion temperature T_i).
Without considering wall emission, when both the positive ions and electrons from the plasma are injected from flux source functions, a discrepancy (roughly 20%) between the source sheath computed in[31] and the analytical results of[32] appears for $T_e/T_i = 0.25$ (see Table 1 of[31]). A good agreement is found for larger values of T_e/T_i, which is typically the case of low temperature plasmas.
When considering wall electron emission, most concerns are related to discrepancies with fluid results (cold ion temperature $T_i = 0$, see[27] for example) are observed[35,36]. When the plasma electron temperature is much larger than the wall emitted secondary electron temperature ratio and for $T_i = 0.1\,T_e$, larger values of the source sheath and lower values of the sheath potential drops than what is found with fluid theories are computed with the present formalism. The reason for these discrepancies is that the Bohm criterion is enforced by a large margin with the present model under the previous temperature conditions. This is a known limitation of the formalism used in this paper.
However and as will be shown below, for comparable species temperatures, a very good agreement is found with fluid theories and particle-in-cell code results, both enforcing the Bohm criterion marginally[2]. Furthermore, it should be stressed that a detailed and rigorous description of the presheath and the Bohm criterion is out of the scope of this paper.

B. Model and assumptions

A one-dimensional region is considered. A planar source located at x_p injects temporally constant equal fluxes in the positive-x direction of positive and negative charges following

a half-Maxwellian distribution: several kind of positive ions, negative ions with different masses and temperatures as well as electrons can be considered. The plasma is bounded by a surface located at x_s. The surface can be floating or biased and can emit negative ions and/or electrons in the negative-x direction i.e. towards the plasma.
With exception of the particles source term, no particle creation or annihilation as well as no collisions are considered between the system boundaries.

The phase-space velocity distribution function of the plasma particles is written $f_p(v_x, v_y, v_z)H(v_x)$ where the Heaviside function H ensures that only particles travelling in the positive-x direction are injected. Because the force applied to any of the injected species is determined only by the electric field and by conservation of the momentum and energy, the initial velocity v_p of a particle injected at x_p is related to its velocity at the position x by the relation

$$v_{px} = \left(v_x^2 + \frac{2[U(x) - U_p]}{m} \right)^{1/2} \tag{1}$$

where $U_p = U(x_p)$ is the particle's potential energy at x_p and m is the particle mass. Charged particle phase-space distributions must satisfy the steady-state Vlasov equation:

$$m v_x \frac{\partial f_x(x, \mathbf{v})}{\partial x} = \frac{\partial U(x)}{\partial x} \frac{\partial f_x(x, \mathbf{v})}{\partial v_x} \tag{2}$$

A solution of (2) is given by $f(x, v_x, v_y, v_z) = f_p(v_{px}, v_y, v_z)$ where v_{px} is replaced by the right-hand side of (1).
Considering that the source emits a half-Maxwellian velocity distribution function, it follows

$$f(p, \mathbf{v})H(v_x) = n_p \left(\frac{\beta}{\pi} \right)^{\frac{3}{2}} e^{-\beta v^2} H(v_x) \tag{3}$$

with $\beta = m/(2T_p)$, and n_p and T_p are the density and temperature (in energy units) associated with the full-Maxwellian velocity distribution $f_p(\mathbf{v})$.

For the surface-emitted particle species, fluxes, velocities etc... are defined positive in the negative-x direction. As a consequence, the previous considerations hold for surface-emitted particles when p $\leftrightarrow$ s.

The first several moments are then derived to obtain the particle density n, particle flux Γ, normalized temperature [1] T / T_p and energy flux Q:

$$n = \int f d^3v \tag{4}$$

$$\Gamma = \int v_x f d^3v \tag{5}$$

$$\frac{T}{T_p} = \frac{2\beta}{3} \left[\frac{\int v^2 f d^3v}{\int f d^3v} - \left(\frac{\int v_x f d^3v}{\int f d^3v} \right)^2 \right] \tag{6}$$

$$Q = \frac{1}{2} \int v^2 v_x f d^3v \tag{7}$$

In the following, eqs. (4-7) are applied to derive the densities, particle fluxes, normalized temperatures and energy fluxes of the different species.

C. Particles description

The relations for the plasma postive ions, plasma electrons and negative ions, secondary electron emission and surface produced negative ions emission are listed below. Most of the Ordonez[17] notations are retained, and described in the following.
Location subscripts: p — edge plasma - source sheath interface, 0 — source sheath - sheath interface, m — potential minimum of the virtual cathode (when it exists), s — sheath - wall interface. The difference in values at two locations is denoted by two adjacent locations subscripts as shown in this example giving the potential difference between the source and the wall: $\phi_{ps} = \phi_p - \phi_s$. Particles subscritps: i — plasma positive ions, e — plasma electrons, i^- — plasma negative ions, e_w — secondary electrons, i_w^- — wall negative ion emission. Symbols: ϕ — electric potential, e — the unit charge. Definitions: $\beta_i = m_i/(2T_i)$, $\beta_e = m_e/(2T_e)$, $\beta_{i^-} = m_{i^-}/(2T_{i^-})$, $\beta_{e_w} = m_{e_w}/(2T_{e_w})$, $\beta_{i_w^-} = m_{i_w^-}/(2T_{i_w^-})$. $\psi_\rho = Z_k q \phi_\rho / T_\rho$ with q the elementary charge and Z_k the ionization state number associated to every particle as illustrated with these two examples: $\psi_{spe} = -e[\phi_s - \phi_p]/T_e$, $\psi_{spi} = Z_k e[\phi_s - \phi_p]/T_i$.
Additionally, one defines the two functions $G_1 = e^x \mathrm{erfc}(\sqrt{x})$ and $G_2 = e^x \mathrm{erfc}(-\sqrt{x})$ where erfc is the complementary error function.

1. Plasma positive ions

For both sub-critical and critical regimes shown in Fig. 1, plasma positive ions are described by

$$f_i(x, \mathbf{v}) = n_{pi} \left(\frac{\beta_i}{\pi} \right)^{\frac{3}{2}} e^{-\beta_i v^2 + \psi_{pxi}} H\left[v_x - \left(\frac{\psi_{pxi}}{\beta_i} \right)^{\frac{1}{2}} \right] \tag{8}$$

$$n_i = \frac{1}{2} n_{pi} G_1(\psi_{pxi}) \tag{9}$$

$$\Gamma_i = \frac{n_{pi}}{2\sqrt{\pi \beta_i}} \tag{10}$$

[1] Because the velocity distribution function of the particles is not Maxwellian any more as soon as they encounter a potential gradient in the absence of collisions, the quantity $\frac{T}{T_p}$ cannot be defined as a normalized temperature strictly speaking. This denomination is however kept by extension of the temperature definition.

$$\frac{T_i}{T_{pi}} = 1 + \frac{2\sqrt{\psi_{pxi}/\pi}}{3G_1(\psi_{pxi})} - \frac{2}{3\pi[G_1(\psi_{pxi})]^2} \tag{11}$$

$$Q_i = \frac{(2+\psi_{pxi})n_{pi}T_{pi}}{2\sqrt{\pi\beta_i}} \tag{12}$$

When considering multiple positive ion species, one defines $\alpha_k = Z_k n_{pi,k}/(Z_1 n_{pi,1})$ with $k > 0$. This corresponds to the normalization of the k-th positive ion density to the first positive ion density.

2. Plasma electrons and negative ions

Considering sub-critical regime (Fig. 1a curve) it follows for the negative ions:

$$f_i^-(x,\mathbf{v}) = n_{pi^-}\left(\frac{\beta_i^-}{\pi}\right)^{\frac{3}{2}} e^{-\beta_i^- v^2 - \psi_{xpi^-}} H\left[v_x + \left(\frac{\psi_{sxi^-}}{\beta_i^-}\right)^{\frac{1}{2}}\right] \tag{13}$$

$$n_i^- = \frac{1}{2} n_{pi^-} e^{-\psi_{spi^-}} G_2(\psi_{sxi^-}) \tag{14}$$

$$\Gamma_i^- = \frac{n_{pi^-} e^{-\psi_{spi^-}}}{2\sqrt{\pi\beta_i^-}} \tag{15}$$

$$\frac{T_i^-}{T_{pi^-}} = 1 - \frac{2\sqrt{\psi_{sxi^-}/\pi}}{3G_2(\psi_{sxi^-})} - \frac{2}{3\pi[G_2(\psi_{sxi^-})]^2} \tag{16}$$

$$Q_i^- = \frac{(2+\psi_{sxi^-})n_{pi^-}T_{pi^-}e^{-\psi_{spi^-}}}{2\sqrt{\pi\beta_i^-}} \tag{17}$$

When considering the critical profile (Fig. 1b curve) and provided $\phi_p \geq \phi_s$, it follows:

$$f_i^-(x,\mathbf{v}) = \begin{cases} n_{pi^-}\left(\frac{\beta_i^-}{\pi}\right)^{\frac{3}{2}} e^{-\beta_i^- v^2 - \psi_{xpi^-}} H\left[v_x + \left(\frac{\psi_{mxi^-}}{\beta_i^-}\right)^{\frac{1}{2}}\right] & x_p \leq x \leq x_m \\ n_{pi^-}\left(\frac{\beta_i^-}{\pi}\right)^{\frac{3}{2}} e^{-\beta_i^- v^2 - \psi_{xpi^-}} H\left[v_x - \left(\frac{\psi_{mxi^-}}{\beta_i^-}\right)^{\frac{1}{2}}\right] & x_m \leq x \leq x_s \end{cases} \tag{18}$$

$$n_i^- = \begin{cases} \frac{1}{2} n_{pi^-} e^{-\psi_{mpi^-}} G_2(\psi_{mxi^-}) & x_p \leq x \leq x_m \\ \frac{1}{2} n_{pi^-} e^{-\psi_{mpi^-}} G_1(\psi_{mxi^-}) & x_m \leq x \leq x_s \end{cases} \tag{19}$$

$$\Gamma_i^- = \frac{n_{pi^-} e^{-\psi_{mpi^-}}}{2\sqrt{\pi\beta_i^-}} \tag{20}$$

$$\frac{T_i^-}{T_{pi^-}} = \begin{cases} 1 - \frac{2\sqrt{\psi_{mxi^-}/\pi}}{3G_2(\psi_{mxi^-})} - \frac{2}{3\pi[G_2(\psi_{mxi^-})]^2} & x_p \leq x \leq x_m \\ 1 + \frac{2\sqrt{\psi_{mxi^-}/\pi}}{3G_1(\psi_{mxi^-})} - \frac{2}{3\pi[G_1(\psi_{mxi^-})]^2} & x_m \leq x \leq x_s \end{cases} \tag{21}$$

$$Q_i^- = \frac{(2+\psi_{mxi^-})n_{pi^-}T_{pi^-}e^{-\psi_{mpi^-}}}{2\sqrt{\pi\beta_i^-}} \tag{22}$$

The previous equations are valid to describe the plasma electrons by $\mathrm{e} \leftrightarrow \mathrm{i}^-$. The plasma electronegativity is defined by $n_{pi^-}/n_{pe} = \alpha_0$.

3. Surface emitted negative ions and electrons

Here is considered the ideal case where the negative ions or electrons hitting the wall are lost (see[38] for example when secondary electrons are not absorbed by the wall).

Surface electron emission (SEE) generally originates from thermionic electron emission or when an electron[39–41] or an ion with sufficient energy strike the surface[42,43]. When considering thermionic electron emission, one can, as done in this paper, approximate the secondary electrons velocity distribution function by a half-Maxwellian because the Richardson-Dushmann equation[44] governing the SEE exhibits a distribution proportional to the surface temperature. When considering secondary electron emission generated by electrons, the velocity distribution is more complex[45].

Concerning the negative ions emitted from a surface, there is an experimental evidence suggesting they are formed with a Maxwellian distribution[46]. For this reason, the negative ions emitted from the wall are also approximated by a

half-Maxwellian distribution.

Considering the case of a sub-critical regime (Fig. 1a curve) it follows for the wall-emitted negative ions

$$f_{i_w^-}^-(x,\mathbf{v}) = n_{si_w^-}\left(\frac{\beta_{i_w^-}^-}{\pi}\right)^{\frac{3}{2}} e^{-\beta_{i_w^-}^- v^2 + \psi_{sxi_w^-}} H\left[v_x - \left(\frac{\psi_{sxi_w^-}}{\beta_{i_w^-}^-}\right)^{\frac{1}{2}}\right] \tag{23}$$

$$n_{i_w^-}^- = \frac{1}{2} n_{si_w^-} G_1(\psi_{sxi_w^-}) \tag{24}$$

$$\Gamma_{i_w^-}^- = \frac{n_{si_w^-}}{2\sqrt{\pi\beta_{i_w^-}^-}} \tag{25}$$

$$\frac{T_{i_w^-}^-}{T_{si_w^-}^-} = 1 + \frac{2\sqrt{\psi_{sxi_w^-}/\pi}}{3G_1(\psi_{sxi_w^-})} - \frac{2}{3\pi[G_1(\psi_{sxi_w^-})]^2} \tag{26}$$

$$Q_{i_w^-}^- = \frac{(2+\psi_{sx_{i_w^-}})n_{si_w^-}T_{i_w^-}}{2\sqrt{\pi\beta_{i_w^-}^-}} \tag{27}$$

Considering the case of a critical (Fig. 1b curve) regime and provided $\phi_p \geq \phi_s$, one has:

$$f_{i_w^-}^-(x,\mathbf{v}) = \begin{cases} n_{si_w^-}\left(\frac{\beta_{i_w^-}^-}{\pi}\right)^{\frac{3}{2}} e^{-\beta_{i_w^-}^- v^2 - \psi_{xsi_w^-}} H\left[v_x - \left(\frac{\psi_{mxi_w^-}}{\beta_{i_w^-}^-}\right)^{\frac{1}{2}}\right] & x_p \leq x \leq x_m \\ n_{si_w^-}\left(\frac{\beta_{i_w^-}^-}{\pi}\right)^{\frac{3}{2}} e^{-\beta_{i_w^-}^- v^2 + \psi_{xsi_w^-}} H\left[v_x + \left(\frac{\psi_{mxi_w^-}}{\beta_{i_w^-}^-}\right)^{\frac{1}{2}}\right] & x_m \leq x \leq x_s \end{cases} \tag{28}$$

$$n_{i_w^-}^- = \begin{cases} \frac{1}{2} n_{si_w^-} e^{-\psi_{msi_w^-}} G_1(\psi_{mxi_w^-}) & x_p \leq x \leq x_m \\ \frac{1}{2} n_{si_w^-} e^{-\psi_{msi_w^-}} G_2(\psi_{mxi_w^-}) & x_m \leq x \leq x_s \end{cases} \tag{29}$$

$$\Gamma_{i_w^-}^- = \frac{n_{si_w^-} e^{-\psi_{msi_w^-}}}{2\sqrt{\pi\beta_{i_w^-}^-}} \tag{30}$$

$$\frac{T_{i_w^-}^-}{T_{si_w^-}^-} = \begin{cases} 1 + \frac{2\sqrt{\psi_{mxi_w^-}/\pi}}{3G_1(\psi_{mxi_w^-})} - \frac{2}{3\pi[G_1(\psi_{mxi_w^-})]^2} & x_p \leq x \leq x_m \\ 1 - \frac{2\sqrt{\psi_{mxi_w^-}/\pi}}{3G_2(\psi_{mxi_w^-})} - \frac{2}{3\pi[G_2(\psi_{mxi_w^-})]^2} & x_m \leq x \leq x_s \end{cases} \tag{31}$$

$$Q_{i_w^-}^- = \frac{(2+\psi_{mxi_w^-})n_{si_w^-}T_{i_w^-}e^{-\psi_{msi_w^-}}}{2\sqrt{\pi\beta_{i_w^-}^-}} \tag{32}$$

The previous equations are also valid for the secondary emitted electrons by $e_w \leftrightarrow i_w^-$.

One defines the wall-emitted flux of secondary electrons by $\Gamma_{e_w} = \delta_e\Gamma_e$ with $\delta_e \in \mathbb{R}^+$.
For wall-emitted negative ions and to keep calculation tractable, it is convenient to define $n_{si_w^-} = \delta_i n_{pi}$ with $\delta_i \in \mathbb{R}^+$. The two parameters δ_e and δ_i are used to set the surface secondary electron and emitted negative ion density.

III. DERIVATION OF THE SHEATH AND SOURCE SHEATH POTENTIAL PROFILES

Several conditions are implemented in order to evaluate the source sheath and sheath potentials, i.e. to determine the values of ϕ_p, ϕ_s and ϕ_m.
The first condition is that the charge density at the sheath-source sheath interface is zero. The second condition is to have a source sheath globally quasi-neutral i.e. that the integral of the charge density in the source sheath is zero. The third condition is that the electric field is zero at the potential minimum when space charge saturation is reached. The third condition thus only applies to the critical sheath regime.

In the following, the model is extended to a general case, including many different particles.

A. Zero charge density at the sheath-source sheath interface

To implement the first condition, one first has to determine the total current density flowing through the wall, which in turn permits to control the regime (floating or current conducting wall) for which the model is used. In the case of multiple plasma positive ion species, it is convenient to normalize the total current density to the first positive ion specie current density. At the wall, the normalized current density defined as

$$\gamma_i = \frac{e\sum_{k=1}^{n} Z_k\Gamma_{i,k} - e\left(\Gamma_e + \Gamma_i^- - \Gamma_{e_w} - \Gamma_{i_w^-}^-\right)}{eZ_1\Gamma_{i,1}} \tag{33}$$

with $\Gamma_{i,k}$ is the kth positive ion specie with kth ionization state. This definition solely depends whether one wants to apply the model near the ion satuation current as done in this paper and in[18] or near the electron saturation current like in[17] where the wall current density was then normalized to eΓ_e. Calculations at the floating potential can be performed by setting $\gamma_i = 0$.

One has then to compute the neutralization factor defined by $\alpha = Z_1 n_{pi,1}/n_{pe}$[25]. For sub-critical regime, substituting eqs. (10), (15) applied to plasma electrons and negative ions, (25) applied to wall-emitted secondary electrons and negative ions into eq. (33) and rearranging, the neutralization factor is

$$\alpha = e^{-\psi_{spe}} \frac{\sqrt{\frac{\beta_{i,1}}{\beta_e}}\left(1-\delta_p+\alpha_0 e^{\psi_{spe}-\psi_{spi^-}}\sqrt{\frac{\beta_e}{\beta_i^-}}\right)}{1+\sum_{k=2}^{n}\alpha_k\sqrt{\frac{\beta_{i,1}}{\beta_{i,k}}}+\delta_i\sqrt{\frac{\beta_{i,1}}{\beta_{i_w}^-}}-\gamma_i} \tag{34}$$

For critical regime and as long as $\phi_p \geq \phi_s$, substituting eqs. (10), (20) applied to plasma electrons and negative ions, (30) applied to wall-emitted secondary electrons and negative ions into eq. (33) and rearranging yields

$$\alpha = e^{-\psi_{mpe}} \frac{\sqrt{\frac{\beta_{i,1}}{\beta_e}}\left(1-\delta_p e^{-\psi_{mse_w}}+\alpha_0 e^{\psi_{mpe}-\psi_{mpi^-}}\sqrt{\frac{\beta_e}{\beta_i^-}}\right)}{1+\sum_{k=2}^{n}\alpha_k\sqrt{\frac{\beta_{i,1}}{\beta_{i,k}}}+\delta_i e^{-\psi_{msi_w^-}}\sqrt{\frac{\beta_{i,1}}{\beta_{i_w}^-}}-\gamma_i} \tag{35}$$

One recovers the relations for α derived in[18] by considering only one positive ion specy and setting $\alpha_0 = 0$ and $\delta_i = 0$ in eqs. (33-35).

The condition of zero charge density is used to match the potential values at the sheath-source sheath interface.
The total charge density

$$\rho = e\left(\sum_{k=1}^{n} n_{i,k} - n_e - n_i^- - n_{e_w} - n_{i_w}^-\right) \tag{36}$$

is needed for this condition.

For the sub-critical regime, using eq. (9), (14) applied to plasma electrons and negative ions, (24) applied to wall-emitted secondary electrons and negative ions and rearranging so that α from eq. (34) appears, it follows

$$\frac{2e^{\psi_{spe}}}{en_{pe}}\rho = \alpha e^{\psi_{spe}}\left[\sum_{k=1}^{n}\alpha_k G_1(\psi_{pxi,k}) - \delta_i G_1(\psi_{sxi_w^-})\right] - G_2(\psi_{sxe}) - \alpha_0 e^{\psi_{spe}-\psi_{spi^-}} G_2(\psi_{sxi^-}) - \delta_p\sqrt{\frac{\beta_{e_w}}{\beta_e}} G_1(\psi_{sxe_w}) \tag{37}$$

For the critical regime, using eq. (9), (19) applied to plasma electrons and negative ions, (29) applied to wall-emitted secondary electrons and negative ions and rearranging so that α from eq. (35) appears, it follows

$$\frac{2e^{\psi_{mpe}}}{en_{pe}}\rho = \alpha e^{\psi_{mpe}}\left[\sum_{k=1}^{n}\alpha_k G_1(\psi_{pxi,k}) - \delta_i e^{-\psi_{msi_w^-}} G_1(\psi_{mxi_w^-})\right] - G_2(\psi_{mxe}) - \alpha_0 e^{\psi_{mpe}-\psi_{mpi^-}} G_2(\psi_{mxi^-}) - \delta_p e^{-\psi_{mse_w}}\sqrt{\frac{\beta_{e_w}}{\beta_e}} G_1(\psi_{mxe_w}) \tag{38}$$

The first condition requires that the right-hand side of the eqs. (37-38) to be zero at x_0 which is written as

$$\alpha e^{\psi_{spe}}\left[\sum_{k=1}^{n}\alpha_k G_1(\psi_{p0i,k}) - \delta_i G_1(\psi_{s0i_w^-})\right] = G_2(\psi_{s0e}) + \alpha_0 e^{\psi_{spe}-\psi_{spi^-}} G_2(\psi_{s0i^-}) + \delta_p\sqrt{\frac{\beta_{e_w}}{\beta_e}} G_1(\psi_{s0e_w}) \tag{39}$$

for the eq. (37), and

$$\alpha e^{\psi_{mpe}}\left[\sum_{k=1}^{n}\alpha_k G_1(\psi_{p0i,k})-\delta_i e^{-\psi_{msi_w^-}}G_1(\psi_{m0i_w^-})\right]=G_2(\psi_{m0e})+\alpha_0\, e^{\psi_{mpe}-\psi_{mpi^-}}G_2(\psi_{m0i^-})+\delta_p e^{-\psi_{mse_w}}\sqrt{\frac{\beta_{e_w}}{\beta_e}}G_1(\psi_{m0e_w}) \quad (40)$$

for the eq. (38).

B. Globally quasineutral source sheath

Ensuring a globally quasineutral source sheath requires that the electric field at x_p and x_0 locations to be zero. This is equivalent of having the spatial integral of the total charge density equal to zero within the source sheath boundaries which can be written as $\int_{\phi_p}^{\phi_0}\rho\,\mathrm{d}\phi=0$ or $\int_{\psi_{pe}}^{\psi_{0e}}\rho\,\mathrm{d}\psi_{xe}=0$. Thus, for the sub-critical regime, using eq. (37) the second condition yields

$$\begin{aligned}\alpha e^{\psi_{spe}}\int_{\psi_{pe}}^{\psi_{0e}}\left[\sum_{k=1}^{n}\alpha_k G_1(\psi_{pxi,k})-\delta_i G_1(\psi_{sxi_w^-})\right]\mathrm{d}\psi_{xe}&=\int_{\psi_{pe}}^{\psi_{0e}}G_2(\psi_{sxe})\,\mathrm{d}\psi_{xe}\\ +\alpha_0 e^{\psi_{spe}-\psi_{spi^-}}\int_{\psi_{pe}}^{\psi_{0e}}G_2(\psi_{sxi^-})\mathrm{d}\psi_{xe}&+\delta_p\sqrt{\frac{\beta_{e_w}}{\beta_e}}\int_{\psi_{pe}}^{\psi_{0e}}G_1(\psi_{sxe_w})\,\mathrm{d}\psi_{xe}\end{aligned} \quad (41)$$

For the critical regime one has, using eq. (38)

$$\begin{aligned}\alpha e^{\psi_{mpe}}\int_{\psi_{pe}}^{\psi_{0e}}\left[\sum_{k=1}^{n}\alpha_k G_1(\psi_{pxi,k})-\delta_i e^{-\psi_{msi_w^-}}G_1(\psi_{mxi_w^-})\right]\mathrm{d}\psi_{xe}&=\int_{\psi_{pe}}^{\psi_{0e}}G_2(\psi_{mxe})\,\mathrm{d}\psi_{xe}\\ +\alpha_0\, e^{\psi_{mpe}-\psi_{mpi^-}}\int_{\psi_{pe}}^{\psi_{0e}}G_2(\psi_{mxi^-})\,\mathrm{d}\psi_{xe}&+\delta_p e^{-\psi_{mse_w}}\sqrt{\frac{\beta_{e_w}}{\beta_e}}\int_{\psi_{pe}}^{\psi_{0e}}G_1(\psi_{mxe_w})\,\mathrm{d}\psi_{xe}\end{aligned} \quad (42)$$

C. Zero electric field at ϕ_m

Enforcing zero electric field at ϕ_m is a condition only valid in the critical regime. The electric field is already zero at the sheath-source sheath interface (first condition, zero charge density at the source-source sheath interface), requiring also a zero electric field at the potential minimum is equivalent to requiring the spatial integral of the charge density between the sheath-source sheath interface and the potential minimum to be zero. Thus it is similar to the second condition except it applies between x_0 and x_m and one has

$$\begin{aligned}\alpha e^{\psi_{mpe}}\int_{\psi_{0e}}^{\psi_{me}}\left[\sum_{k=1}^{n}\alpha_k G_1(\psi_{pxi,k})-\delta_i e^{-\psi_{msi_w^-}}G_1(\psi_{mxi_w^-})\right]\mathrm{d}\psi_{xe}&=\int_{\psi_{0e}}^{\psi_{me}}G_2(\psi_{mxe})\,\mathrm{d}\psi_{xe}\\ +\alpha_0 e^{\psi_{mpe}-\psi_{mpi^-}}\int_{\psi_{0e}}^{\psi_{me}}G_2(\psi_{mxi^-})\,\mathrm{d}\psi_{xe}&+\delta_p e^{-\psi_{mse_w}}\sqrt{\frac{\beta_{e_w}}{\beta_e}}\int_{\psi_{0e}}^{\psi_{me}}G_1(\psi_{mxe_w})\,\mathrm{d}\psi_{xe}\end{aligned} \quad (43)$$

The integrals from eqs. (41-43) can be evaluated provided the two indefinite integrals (44-45)

$$\int G_1(x)dx = G_1(x) + 2\left(\frac{x}{\pi}\right)^{\frac{1}{2}} \tag{44}$$

and

$$\int G_2(x)dx = G_2(x) - 2\left(\frac{x}{\pi}\right)^{\frac{1}{2}} \tag{45}$$

as well as $\psi_i = -Z_i\psi_e T_{pe}/T_{pi}$, $\psi_{i_w^-} = \psi_e T_{pe}/T_{pi_w^-}$, $\psi_{i^-} = \psi_e T_{pe}/T_{pi^-}$ and $\psi_{e_w} = \psi_e T_{pe}/T_{pe_w}$

D. Solution for ϕ_p, ϕ_m, ϕ_s and potential profile

The electric potential at one location has to be defined. One chooses to define the sheath-source sheath interface potential as zero, $\psi_{0e} = 0$. With $\psi_{0e} = 0$, for the sub-critical regime, eqs. (39) and (41) are solved simultaneously for the two unknowns ϕ_p and ϕ_s. For the critical regime, eqs. (40), (42) and (43), are solved simultaneously for the three unknowns ϕ_p, ϕ_m and ϕ_s respectively.
Furthermore, the onset of space-charge saturation which corresponds to the transition between sub-critical to critical regimes can be found by solving eqs. (40), (42) and (43) for ϕ_p, ϕ_s and either δ_i or δ_p under the condition $\phi_m = \phi_s$. Once the values of the potentials ϕ_p, ϕ_m and ϕ_s are known, the potential profile can be computed by solving the Poisson equation

$$\Delta\phi = -\frac{\rho}{\varepsilon_0} \tag{46}$$

E. Determination of the depth of the potential well

When the surface emitted current of secondary electrons or negative ions is larger than the critical value δ_c, a potential well appears to limit the transported current from the surface towards to plasma to the critical value. The depth of the potential well can be evaluated as in[50], in the simplest case where only secondary electrons or negative ions are emitted from the wall by equating eq. (25) and eq. (30). It follows

$$\phi_s - \phi_m = T_p \times ln\left(\frac{\delta}{\delta_c}\right) \tag{47}$$

for $\delta > \delta_c$ and T_p being the temperature either of secondary electrons or negative ions.

IV. PARTICLE-IN-CELL

The one-dimentional PIC code BACON[21] is used to benchmark the present analytical results. Only the main properties of this code will be recalled here as it was already presented[21] and benchmarked[51]. This code permitted to model the sheath using typical plasma parameters for a hydrogen plasma in a negative hydrogen ion source[21].

The calculation domain consists in a particle source facing a wall. At the particle source, equal numbers of positive ions and electrons are injected each time steps in both directions. The absolute numbers of injected particles are determined and adjusted according to particle densities in the plasma volume defined in the code input. All three velocity components are included. The initial velocity is determined randomly according to a Maxwellian flux velocity distribution function[31]. At the wall, where Dirichlet boundary conditions are used, negative ions are injected towards the plasma. Monte Carlo routine are used to compute the flux of the injected negative ions generated by neutrals and positive ions hitting the wall.
Positive ions and electrons crossing the position of the particle source are started again with new random velocity and direction. This procedure ensures quasi-neutrality in the bulk plasma and represents thermalization of the particles by collision processes. Negative hydrogen ions which cross the particle source are destroyed. Around the particle source a source sheath evolves, which ensures quasi-neutrality in the calculation domain.
Collisions between particles are not considered because the size of the calculation domain (300 μm) is much smaller than the mean free path of electrons and ions, the typical Debye length being around 30 μm for an electron density of $10^{17}\,m^{-3}$ and a temperature of 2 eV.
The typical execution time of BACON is 1 hour per run, while less than one second is required for the presented model.

V. COMPARISON OF ANALYTICAL AND PARTICLE-IN-CELL RESULTS

For the simplest case of an electropositive hydrogen plasma with one positive ion specie (protons), potential sheath drops and sheath sizes of the presented analytical model were successfully benchmarked in[51] against two particle-in-cell codes ONIX[52,53] and BACON[21] and one analytical model[28]. Both ONIX and BACON enforce the Bohm criterion and the presheath voltage drop within 20 % when compared to fluid sheath results.

Here, the analytical model is benchmarked against BACON in the case of two positive ion species, protons and caesium ions, and with negative hydrogen ions emitted from the wall as an example case for a negative hydrogen ion source and the densities, temperatures and all ion species have been chosen according to what was measured[54]. The use of the analytical model is suited for this case because the temperatures of the species are comparable as shown below. Figure 2 compares the potential profiles ϕ, plasma electrons densities n_e, positive ion densities n_{H^+} and n_{Cs^+} for protons and caesium respectively, as well as surface emitted negative hydrogen ions n_{H^-} for $T_e = 2$ eV, $T_{H^+} = T_{Cs^+} = T_{H^-} = 0.8$ eV obtained analytically and with PIC code for two different wall negative ion density: a) $8.3\text{x}10^{17}\,m^{-3}$ and b) $2\text{x}10^{18}\,m^{-3}$, taken from[21]. The comparison between the analytical and PIC results was performed, for both Figures 2 a) and b), as follows:

- at the plasma side i.e. $3\text{x}10^{-4}$ m, the densities of

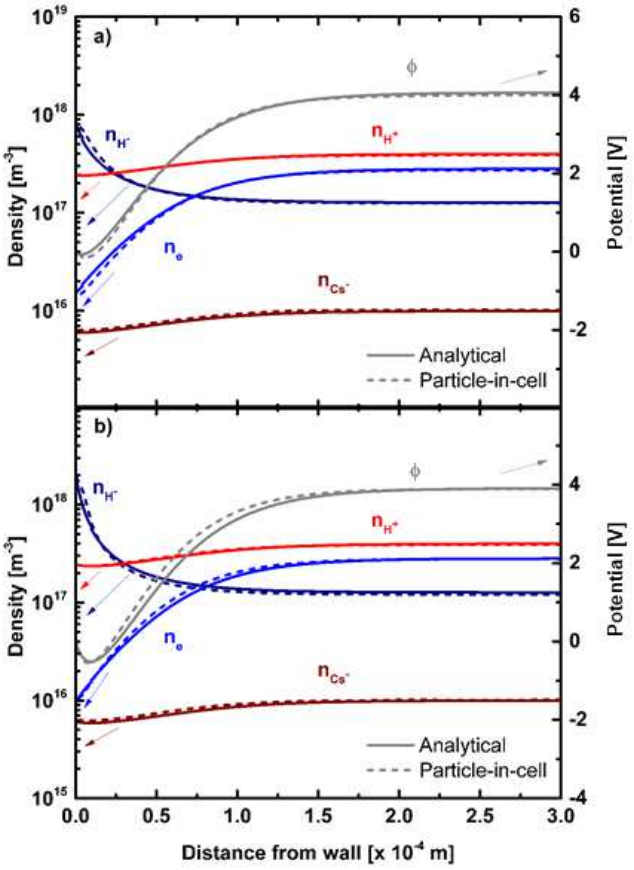

FIG. 2. Comparison of the potential profiles ϕ, plasma electrons densities n_e, positive ion densities n_{H^+} and n_{Cs^+} as well as surface emitted negative ions n_{H^-} for $T_e = 2$ eV, $T_{H^+} = T_{Cs^+} = T_{H^-} = 0.8$ eV obtained analytically and with PIC code[21] for a wall negative ion density of: a) $8.3\text{x}10^{17}$ m^{-3} and b) $2\text{x}10^{18}$ m^{-3}. The wall and plasma are located at 0 and $3\text{x}10^{-4}$ m respectively.

the two positive ion species ($n_{H^+} = 4\text{x}10^{17}$ m^{-3} and $n_{Cs^+} = 1\text{x}10^{16}$ m^{-3}), temperatures of the aforementioned species (and electron temperature only) as well as potential values of the analytical model are matched to the PIC results,

- the negative ion densities and temperatures (given before) are matched to the PIC values at the wall side i.e 0 m in Figure 2, while the electron density is calculated self-consistently along the complete domain.

A very good agreement is found between PIC and analytical results for both cases. The dimensions of the sheath and in particular the depth of the potential well and the potential on the plasma side are accurately reproduced by the analytical model. Furthermore, for both graphs shown in Figure 2, the negative ion density computed in the plasma volume is identical. This means that the presented analytical model can describe the space charge limited regime and accurately reproduce the amount of negative ions transported across the sheath.

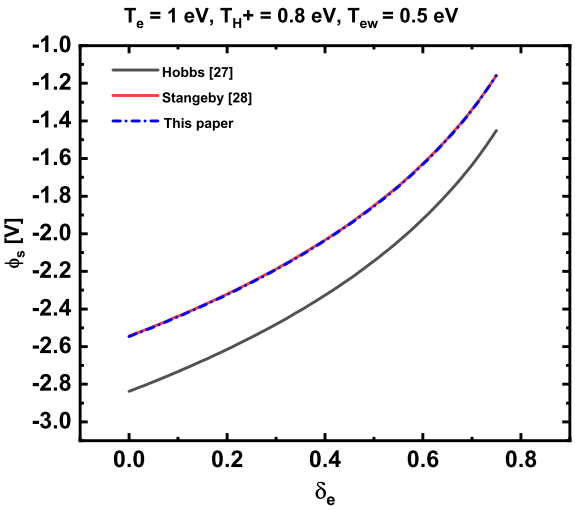

FIG. 3. Variation of the surface floating potential ϕ_s when secondary electron emission is increased for a proton - electron plasma with $T_e = 1$ eV, $T_{H^+} = 0.8$ eV and $T_{e_w} = 0.5$ eV. A comparison of the surface potential found in this paper is made with the analytical relations derived by Hobbs[27] and Stangeby[28].

VI. INFLUENCE OF THE SECONDARY EMISSION AND NEGATIVE ION YIELD ON POTENTIALS AND PARTICLE FLUXES

Figure 3 shows the variation of the floating surface potential ϕ_s when secondary electron emission is increased for a proton - electron plasma with $T_e = 1$ eV, $T_{H^+} = 0.8$ eV and $T_{e_w} = 0.5$ eV, values which are typical of what has been measured in negative hydrogen ion sources for fusion[54]. A comparison between the results found in this paper is made with the analytical relations derived in their paper by Hobbs[27] and Stangeby[28]. For the chosen parameters, an excellent agreement is found between the results obtained in this paper and the analytic solution proposed by Stangeby although fluid formalism is used. A discrepancy increasing to -25% is observed when increasing the electron temperature to 5 eV with the present formalism and Stangeby relation (not shown here). A reasonable agreement is shown also in Figure 3 with between Hobbs relation and the presented results with a maximum of -20% discrepancy.

In Figure 4, another comparison is made with Stangeby and Hobbs analytical results, with the exception that one considers a plasma composed of 40% H^+, 40% H_2^+, 20% H_3^+ and electrons with $T_e = 1$ eV, $T_{H^+} = T_{H_2^+} = T_{H_3^+} = 0.8$ eV and $T_{e_w} = 0.5$ eV for the secondary electrons. The positive ion proportion is equivalent to an effective ion mass of 1.8 a.m.u. and was chosen according to what was previously measured[58]. The effective mass of 1.8 a.m.u. is used in the

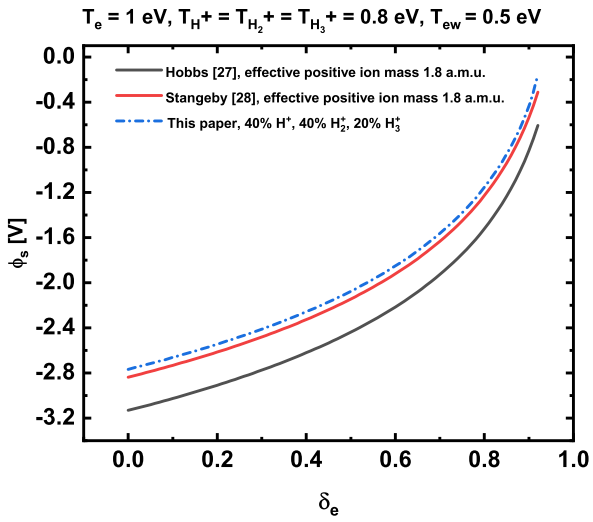

FIG. 4. Variation of the surface floating potential ϕ_s when secondary electron emission is increased for a plasma made of 40% H^+, 40% H_2^+, 20% H_3^+ and electrons with $T_e = 1$ eV, $T_{H^+} = T_{H_2^+} = T_{H_3^+} = 0.8$ eV and $T_{e_w} = 0.5$ eV. A comparison of the surface potential found in this paper is made with the analytical relations derived by Hobbs[27] and Stangeby[28] with a positive ion effective mass of 1.8 a.m.u. corresponding to the plasma composition.

Stangeby and Hobbs relations to derive the floating potential. One observes in Figure 4 a minor difference between the presented results and Stangeby relation using the effective positive ion mass. Furthermore a reasonable agreement is also found with Hobbs analytical relation.

Figure 5a) shows the variation of the positive ion, plasma electrons and the corresponding emitted negative hydrogen ions or secondary electron fluxes, while b) presents the corresponding variation of the surface floating potential ϕ_s, source sheath potential ϕ_p and potential well minimum ϕ_m as function of secondary electron emission or wall-emitted negative hydrogen ions for a plasma made of protons and electrons with $T_e = 1$ eV, $T_{H^+} = 0.8$ eV, $T_{H_w^-} = T_{ew} = 0.5$ eV and for a source positive ion density of 1.9×10^{17} m^{-3}. Dash-dotted and full lines correspond to results obtained with secondary electron emission and wall negative hydrogen ion emission respectively. The labels 1 show the transition between a sub-critical to a critical sheath regime.

In Figure 5a), an increase of δ_e or δ_i leads to an increase of the secondary electron and negative ion fluxes transported across the sheath, as well as an increase of the plasma electron flux directed towards the wall, both until the critical regime is reached. The increase of the plasma electron flux is simply due to the potential difference between the source and the wall being further reduced for both increasing values of the secondary electrons and wall emitted negative ion yields. In Figures 5, the different values for δ_e and δ_i triggering the critical regime are correlated with the mass (electrons or negative ions) but also and very importantly to the different definition

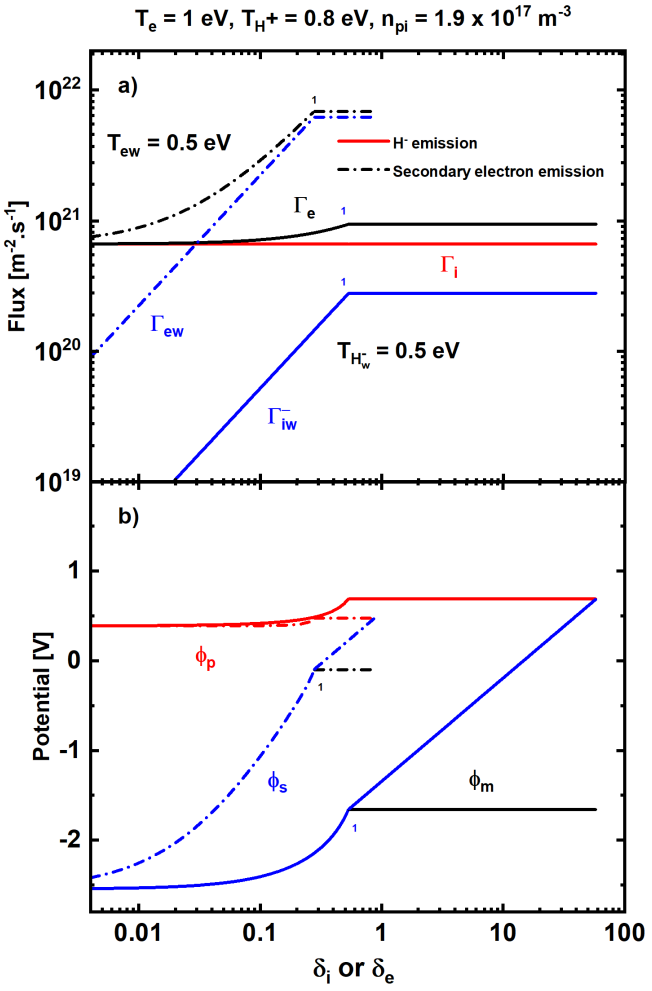

FIG. 5. a): variation of the positive ion, plasma electrons and the corresponding emitted negative hydrogen ions or secondary electron fluxes, b): variation of the surface floating potential ϕ_s, source sheath potential ϕ_p and potential well ϕ_m minimum as function of secondary electron emission or wall-emitted negative hydrogen ions for a plasma made of protons and electrons with $T_e = 1$ eV, $T_{H^+} = 0.8$ eV, $T_{H_w^-} = T_{ew} = 0.5$ eV and for a source positive ion density of 1.9×10^{17} m^{-3}. Dash-dotted and full lines correspond to results obtained with secondary electron emission and wall negative hydrogen ion emission respectively. The labels 1 show the transition between a sub-critical to critical sheath regime.

of δ_e and δ_i (see paragraph II-C-3).

Once the critical regime is reached a saturation of the transported negative ion or secondary electron flux is observed with a further increase of δ_e and δ_i: the potential difference between the wall ϕ_s and the minimum potential well ϕ_m self-adjust to repel towards the wall any exceeding negative charges, as many times observed and commented[15–21]. One also observes in Figure 5a) that the flux of positive ions hitting the wall is constant whatever the values of δ_e and δ_i are. This is to be expected, as in absence of collisions, as long as $\phi_p > \phi_s$, the conservation of the flux imply this result (the positive ion flux for secondary electron emission and wall negative

ion emission superimpose in Figure 5a). The same reasoning hold for the observation of a constant plasma electron flux hitting the wall when the critical regime is reached: the retarding potential for the plasma electrons is ϕ_p - ϕ_m which is a constant, thus there again, as long as $\phi_p > \phi_s$, the conservation of the flux imply a constant plasma electron flux. The maximum values for δ_e and δ_i, under the present chosen parameters are 0.87 and 57.54 respectively, and correspond to the point where $\phi_p = \phi_s$, which is the upper boundary value for the validity domain of the critical regime equations.

VII. CAMPANELL'S INVERSE SHEATH THEORY

Recently, Campanell and colleagues modelled an argon plasma and showed that for very strong secondary electron emission (critical regime), a charge exchange collision occuring in the potential well between a fast positive argon ion coming from the plasma and a room temperature Ar atom led to positive ions being trapped inside the potential well. The accumulation of trapped positive ions reduce the potential well depth until an inverse sheath appears[29,30]. In the Campanell papers, the calculation are made for an electron density in the range of $10^{13}\,\mathrm{m}^{-3}$ for which the potential well and sheath dimensions are in the range of mm and cm respectively as shown in[30]. Furthermore, taking from[30] the charge-exchange cross section $5.5\mathrm{x}10^{-19}\,\mathrm{m}^2$ and the assumed neutral densities ranging from $4.5\mathrm{x}10^{19}\,\mathrm{m}^{-3}$ to $10.5\mathrm{x}10^{19}\,\mathrm{m}^{-3}$ yields a mean free path for the charge exchange collisions ranging from 1.7 to 4 cm which is in the range of the potential well and sheath size.

However, in the case of powerful negative hydrogen ion sources, and as shown in Figure 2, the sheath dimentions are in the order of one to two hundred micrometer and the potential well in the order of tens of micrometers. Furthermore, the charge exchange collision for a proton with a neutral background hydrogen atom is[57] $4\mathrm{x}10^{-19}\,\mathrm{m}^2$ and the neutral background density ranges from[59] $2\mathrm{x}10^{18}\,\mathrm{m}^{-3}$ to $5\mathrm{x}10^{19}\,\mathrm{m}^{-3}$, yielding a mean free path comprised between 5 cm to 1.2 m, greatly exceeding the sheath and potential well dimentions. As a consequence, the possibility of having trapped positive ions in the potential well of a negative hydrogen ion source for the aforementioned plasma parameters is low. The results shown by Campanell are very interesting and the possibility of having an inverse sheath in negative hydrogen ion sources will be thoroughly investigated in detail in a forthcoming paper.

VIII. CONCLUSION

A one-dimensional model of the sheath in front of the wall that emits negative charges has been developed. It is an extension of the work of Ordonez for which many plasma and wall emitted particles species can be taken into account. The equations for a general case, i.e. including several species of positive and negative ions as well as electrons in the bulk together with secondary electron and negative ion surface emission have been derived. A very good agreement between the model, PIC simulations and an analytical model has been demonstrated for the example of negative hydrogen ion sources for fusion. A limitation of the model is that the temperatures of the species have to be comparable.

IX. REFERENCES

[1] Langmuir I., Phys. Rev. 33 (1929) 954.
[2] Bohm, D. 1949 Characteristics of Electrical Discharges in Magnetic Fields (ed. A. Guthrie and R. K. Wakerling), Chap. 3. McGraw-Hill, New York.
[3] Boyd R. L. F. and Thompson J. B., Proc. R. Soc. Lond. 252 (1959) 102.
[4] Prewett P. D. and Allen J. E., Proc. R. Soc. Lond. A348 (1976) 435.
[5] Ordonez C. and Peterkin R. E. Jr., J. Appl. Phys. 79 (1996) 2270.
[6] Cimino R., Collins I. R., Furman M. A., Pivi M., Ruggiero F, Rumolo G. and Zimmermann F., Phys. Rev. Lett. 93 (2004) 014801.
[7] Cimino R., Nucl. Instrum. Methods Phys. Res. A 561 (2006) 272.
[8] Dunaevsky A., Raitses Y. and Fisch N. J., Phys. Plas. 10 (2003) 2574.
[9] Jolivet L. and Roussel J. F., IEEE Trans. Plasma Sci. 30 (2002) 318.
[10] Takamura S., Ohno N., Ye M. Y. and Kuwabara T., Contrib. Plasma Phys. 44(1–3) (2004) 126–137.
[11] Taccogna F., Longo S. and Capitelli M., Phys. Plasmas 11 (2004) 1220.
[12] Franzen P. et al., Nucl. Fus. 47 (2007) 264.
[13] Schiesko L. et al., Plas. Phys. & Cont. Fus. 53 (2011) 085029.
[14] Franzen P., Fantz U., Wünderlich D., Heinemann B., Riedl R., Kraus W., Fröschle M., Ruf B., Nocentini R. and the NNBI Team, Nucl. Fusion 55 (2015) 053005.
[15] Amemiya H., Annaratone H and Allen J. E., J. Plasma Phys. 60 (1998) 81.
[16] Schwager L. A. , Phys. fluids B 5 (1993) 631.
[17] Ordonez C., Phys. Rev. E 55 (1997) 1858.
[18] Stephens K. F. and Ordonez C., Journ. App. Phys. 85 (1999) 2522.
[19] Gyergyek T. and Kovačič J., Contrib. Plasma Phys. 52, (2012) 699.
[20] McAdams R., Holmes A. J. T., King D. B. and Surrey E., Plasma Sources Sci. Technol. 20 (2011) 035023.
[21] Wünderlich D., Gutser R. and Fantz U., Plasma Sources Sci. Technol. 18 (2009) 045031.
[22] Auer P., J. Appl. Phys. 31 (1960) 2096.
[23] McIntyre R. G., J. Appl. Phys. 33 (1962) 2485.
[24] Kuhn S., Plasma Phys. 23 (1981) 881.
[25] Schwager L. A. and Birdsall C. K., Phys. fluids B 2 (1990) 1057.
[26] Nicolai A. and Fuchs G., Journ. Nucl. Mater. 76-77 (1978) 556.
[27] Hobbs G. D. and Wesson J. A., Plasma Phys. 9 (1967) 85.
[28] Stangeby C., Phys. Fluids 27 (1984) 682.
[29] Campanell M. D. and Umansky M. V., Phys. Rev. Lett 116 (2016) 085003.
[30] Campanell M. D. and Umansky M. V., Plasma Sources Sci. Technol. 26 (2017) 124002.
[31] Procassini R. J., Birdsall C. K. and Morse E. C., Phys. Fluids B: Plasma Physics 2 (1990) 3191.
[32] Emmert G. A., Wieland R. M., Mense A. T., and Davidson J. N., Phys. Fluids 23 (1990) 803.
[33] Bissel R. C. and Johnson P. C., Phys. Fluids 30 (1987) 779.
[34] Scheuer J. T. and Emmert G. A., Phys. Fluids 31 (1988) 3645.
[35] Sheehan J. P., Hershkowitz N., Kaganovich I. D., Wang H., Raitses Y., Barnat E. V., Weatherford B. R. and Sydorenko D., Phys. Rev. Lett. 111 (2013) 075002.
[36] Sheehan J. P., Kaganovich I. D., Wang H., Sydorenko D., Raitses Y. and Hershkowitz N., Phys. Plas. 21 (2014) 063502.
[37] Taccogna F., Longo S. and Capitelli M., Phys. Plas. 12 (2005) 093506.
[38] Schiesko L., Carrère M., Cartry G. and Layet J.-M., Phys. Plas. 15 (2008) 073507.
[39] Schupfer N., Tskhakaya D. D., Khanal R., Kuhn S., Aumayr F., da Silva S. F. and Winter H. P., Plasma Phys. Controlled Fusion 48 (2006) 1093.
[40] Taccogna F., Longo S., Capitelli M. and R. Schneider, Contrib. Plasma Phys. 46 (2006) 781.
[41] Raitses Y., Staack D., Keidar M. and Fisch N. J., Phys. Plas. 12 (2005) 057104.
[42] Li X. C. and Wang Y. N., Thin Solid Films 506–507 (2006) 307.

[43]Chapman B., Glow Discharges Processes, Wiley-Interscience, New York (1980).
[44]Herring C. and Nichols M. H., Rev. Mod. Phys. 21 (1949) 185.
[45]Hachenberg O. and Brauer W., Adv. Electron El. Phys. 11 (1959) 413.
[46]Melnychuk S. T., Seidl M., Carr W., Isenberg J. and Lopes J., J. Vac. Sci. Technol. A 7 (1989) 2127.
[47]Baglin V., Collins I., Henrist B., Hilleret N. and Vorlaufer G., LHC project report 472 (2002).
[48]Ordonez C. A. and Peterkin R. E. Jr., J. Appl. Phys. 79 (1996) 2270.
[49]Ordonez C. A., Phys. fluids B 4 (1992) 778.
[50]Gyergyek T. and Kovačič J., Contrib. Plasma Phys. 53, No.3, (2013) 189-201.
[51]Wünderlich D., Mochalskyy S., Montellano I.M. and Revel A., Rev. Sci. Instrum. 89 (2018) 052001.
[52]Mochalskyy S., Fantz U., Wünderlich D. and Minea T., Nucl. Fusion 56 (2016) 106025.
[53]Revel A., Mochalskyy S., Montellano I. M., Wünderlich D., Fantz U. and Minea T., J. Appl. Phys. 122 (2017) 103302.
[54]Heinemann B. et al, New J. Phys. 19 (2017) 015001.
[55]McNeely P., Dudin S. V., Christ-Koch S. and Fantz U.,Plasma Sources Sci. Technol. 18 (2009) 014011.
[56]Schiesko L., McNeely P., Franzen P., Fantz U. and the NNBI Team, Plasma Phys. Control. Fusion 54 (2012) 105002.
[57]Wade L. Fite, Thodore Brackmann R. and William R. Snow, Phys. Rev. 112 (1958) 1161.
[58]Fantz U., Private Communication.
[59]Briefi S., Private Communication.